2021 43rd Annual International Conference of the
IEEE Engineering in Medicine & Biology Society (EMBC)
Oct 31 - Nov 4, 2021. Virtual Conference

# 2D Ultrasound Validation to Assess the Accuracy of Hip Displacement Measurement: A Phantom Study

Thanh-Tu Pham, Thanh-Giang La, Lawrence H. Le, John Andersen, and Edmond Lou, *Member*, IEEE

*Abstract*— **Hip displacement is a common orthopedic abnormality in children with cerebral palsy and is assessed on anteroposterior pelvic radiographs during surveillance. Repeated exposure to ionizing radiation is a major concern of cancer risks for children. Ultrasound (US) has been proposed to image the hips. The severity of hip displacement is measured by the Reimers' migration percentage (MP), which is calculated by the ratio of the femoral head distance from the acetabulum to the width of the femoral head. Methods have been published to estimate MP from the US hip images in literature; however, validation for accuracy has not been reported. This study aimed to determine the accuracy of the 2D ultrasound techniques using two 3D printed hip phantoms with known MP values. The MPs estimated from the US images were compared with those measured from the X-ray images. Based on the experimental results, the US measurements had a maximum absolute discrepancy of 2.2% as compared to 9.8% from the X-ray measurements for the MP. The study on phantoms has showed the proposed US approach is promising with better accuracy and without ionizing radiation.**

*Clinical Relevance* — **If the accuracy is proved to be at least as good as the current X-ray gold standard, the proposed US method will provide a modality of choice to pediatric patients for hip displacement diagnostics and hip surveillance, especially those with cerebral palsy. The method will be free of ionizing radiation and therefore significantly improve the pediatric patient care.**

## I. Introduction

Children with cerebral palsy (CP) experience functional limitations attributed to nonprogressive and permanent damage of the developing brain [1]. The resulting impairments in movement and posture are associated with an elevated risk for developing progressive musculoskeletal anomalies over time. Hip displacement is a common orthopedic abnormality in children with CP, affecting one in three children of this population [2]. The displacement is diagnosed with the femoral head lying beyond the edge of the acetabulum, leading to hip pain and reduced health-related quality of life [3], [4].

Hip surveillance is an effective practice to monitor the hip displacement for children with CP. The goal of surveillance is to identify progressive hip displacement at early stage, thus enabling timely intervention and orthopedic management to reduce pain and maintain flexible hips [5]. Currently, X-ray is the gold standard to image hip displacement. The examination is performed with the patient lying on the back in the supine position and X-ray beam passing from the front to the back (anteroposterior or AP). The amount of hip displacement is assessed by the Reimers' migration percentage (MP), which measures the proportion of the femoral head (FH) uncovered by the acetabulum, known as the head distance to the FH width [6] (Fig. 1(a)). However, cumulative radiation exposure from hip surveillance increases cancer risks for pediatric patients. Although using the low dose X-ray EOS imaging system (EOS imaging, France) and magnetic resonance imaging (MRI) can minimize ionizing exposure, limited accessibility, incapability to acquire supine imaging by EOS, and the need for sedation when using MRI to avoid patient motion have limited their use. Known for its wide availability and lack of ionizing radiation, ultrasound has been considered as an alternate imaging modality for hip surveillance in young children.

Ultrasonography uses mechanical waves and the echoes from the tissue interfaces to image the internal structures noninvasively. Fig. 1(b) and 1(c) show examples of the US coronal and sagittal images of the hip of a 5-year-old volunteer with the parental consent. Pioneer works have demonstrated that US images showed the edges of the acetabulum and the femoral head [7], [8]. However, the MP measurements were not provided in early works due to inability to measure FH width from the US images. Recently Kay et al. used 3D ultrasound to quantify hip displacement and was able to estimate the FH width by manually fitting a circle to the 2D US FH image and assuming the diameter as the FH width [9]. They further proposed an index (1-MPUS) where MPUS is the US-equivalent MP, and found the index correlated strongly with the traditional X-ray based MP.

3D imaging is the most ideal technology to image hip displacement as the volumetric scan provides 3D data volume, which allows image reconstruction at any angle of view. However, the 3D US systems are very expensive and are not very common in most US clinics, especially in the rural areas. Therefore, developing US techniques using conventional 2D probe accompanied with reconstruction algorithms to assess hip displacement could improve access to hip surveillance for children with CP.

The objective of this study was to evaluate the accuracy of measuring MP using 2D US images by validating the US

Research supported by the Glenrose Rehabilitation Hospital Foundation.

T. T. Pham, T.-G. La, and L. H. Le are with the Department of Radiology and Diagnostic Imaging, University of Alberta, Edmonton, AB T6G 2B7, Canada (email: tu.pham@ualberta.ca, thanhgia@ualberta.ca, respectively).

L. H. Le is with the Department of Radiology and Diagnostic Imaging, University of Alberta, Edmonton, AB T6G 2B7, Canada (corresponding author; e-mail: lawrence.le@ualberta.ca).

J. Andersen is with the Department of Pediatrics, University of Alberta, Edmonton, AB T6G 1C9, Canada (e-mail: john.andersen@ahs.ca).

E. H. Lou is with the Department of Electrical and Computer Engineering, University of Alberta, Edmonton, AB T6G 1H9, Canada (corresponding author; e-mail: elou@ualberta.ca).

method using 3D printed hip phantoms with known displacement. In addition, the accuracy of the X-ray method was also studied.

## I. Materials and Methods

### A. *Hip Displacement Phantom*

A right hip phantom of a 5-year-old child consisting of pelvis and femur (Bone Clones Inc., Chatsworth, CA) was scanned by a handheld 3D structure sensor (Occipital, San Francisco, CA) to obtain the 3D digital model. The 3D model was then modified using the AutoDesk Fusion 360 software (Autodesk, San Rafatel, CA) to design the amount of head displacement and the FH width. The phantom was configured to sit on the flat base and allow ultrasound scanning in the sagittal and coronal directions, equivalent to the ultrasound scanning orientation performed on a patient lying supine (see Fig. 2). Two phantoms, namely phantom 1 and phantom 2, were printed with the Polylactic acid (PLA) filament by a Prusa i3 MK3S 3D-printer (Prusa Research, Prague). The printer had a post-printing accuracy of ± 0.15% (± 0.5 mm). The reflection coefficient of the PLA-water interface was approximately 0.1 and weaker than that of bone-soft tissue interface, which ranges from 0.3 to 0.4 [10]. For phantom 1, two beads were used as markers to indicate the acetabular margin and lateral aspect of the femoral head (Fig. 2). The purpose was to highlight the reference landmarks for manual measurements. Phantom 2 was printed with smaller head distance and similar FH width but without markers. The head distance and the FH width of the two phantoms were manually measured on the 3D models using the AutoDesk Fusion 360 measuring tool. The measurements were listed in Table 1.

### B. *Experimental Setup and Data Acquisition*

A hand-held wireless Clarius C3 US scanner (Clarius Mobile Health, Vancouver, BC) was used to scan the hip phantoms. The scanner has an operating frequency range from 2 to 6 MHz. The scanning was performed at 4 MHz and 6 cm

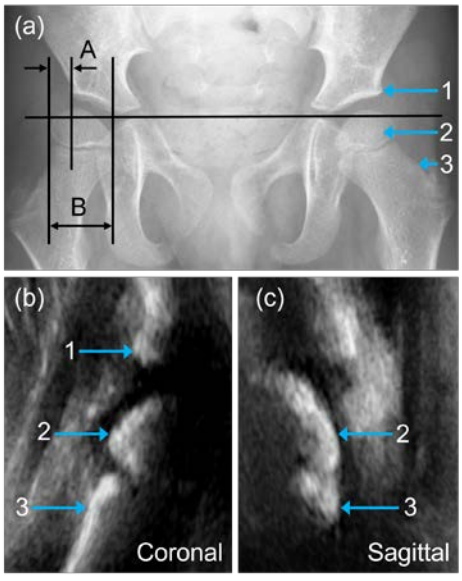


Figure 1. (a) An anteroposterior (AP) pelvic radiograph showing the head distance (A) and femoral head width (B). The US hip images of a 5-year-old child: (b) coronal view and (c) sagittal view. The annotation is as follows: 1. acetabular margin, 2. femoral head, 3. femur.

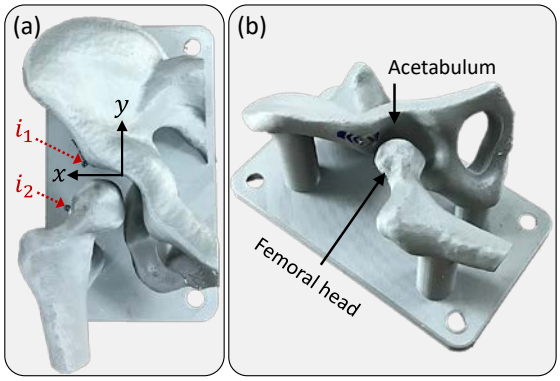


Figure 2. Hip phantom 1: (a) Top view showing two markers, $i_1$ and $i_2$, as denoted by the red arrows; (b) Angle view showing the acetabulum (socket) and the femoral head.

imaging depth using musculoskeletal mode. The distance between the surface of the transducer to the femoral head was set at 2 cm, to mimic the soft tissue thickness overlying the hip. All US scans were performed with the phantoms immersed in a water tank and the transducer head just below the water surface.

Two US scans were performed for each phantom. The first was the coronal scan and was performed with the long axis of the transducer array parallel to the superior-inferior axis of the hip ($y$-axis in Fig. 2(a)) and over the lateral side of the hip joint. The second was the sagittal scan over the anterior side of the hip joint. The sagittal image with the maximum cross section of the femoral head was used to estimate the FH width.

The AP X-ray images of the phantoms were also taken so that the MP values calculated from the X-ray images were evaluated for accuracy.

### C. *Feature Identification*

The head distance, A, is the distance between the lateral acetabular margin ('annotation 1' in Fig 1(a)) and the lateral aspect of the FH. For the hip phantom, the acetabular margin is determined at the midpoint of the lateral curvature of the acetabular roof, as indicated by the marker $i_1$ (Fig. 2(a)), while the lateral aspect of the FH is the lateral border of the femoral head, as shown by the marker $i_2$ (Fig. 2(a)).

### D. *MP Calculation on the Ultrasound Image*

In this study, the head distance, A, was best measured in the coronal view while the FH width, B, was estimated in the sagittal view. The estimation of B was achieved by fitting a circle to the partial imaged femoral head, and then using its diameter as an estimate of B. The MP calculation was obtained by taking percentage of the ratio of the measured A by the estimated B, i.e., $\mathrm{MP} = \mathrm{A}/\mathrm{B} \times 100\%$.

### E. *Image Processing*

*Image Preprocessing*

The acquired US images were exported to an Intel i5 personal computer with 16 GB RAM for further analysis. The images were plotted with proper window and level adjustment to enhance visualization. Regions of interest (ROI) were selected in both views. While the image in the coronal view was directly used to measure A, the ROI cropped from the sagittal view was used for the following processing steps to estimate B.

*Edge Detection*

The FH surface was detected on the selected US sagittal image prior to circle fitting. The image intensities were normalized, and the surface was detected by thresholding. Threshold was set based on the intensity profile across the image of the femoral head. With a proper cutoff, two edges would be detected: one corresponding to the front edge and the other to the back edge, which is due to the ringing effects of the wavelet.

*Circle Fitting*

The set of points thus acquired, $\mathbf{\Gamma}$ were assumed to resemble an arc of a circle. Taubin's method [11], [12] was implemented to optimize the fitting of $n$ points to a circle by minimizing the parametric function in terms of the unknown coefficients, $(P_1, P_2, P_3, P_4)$,

$$F = \sum_{i=1}^{n} (P_1 z_i + P_2 x_i + P_3 y_i + P_4)^2 , \quad (1)$$

subject to the following constraint

$$4P_1^2 \bar{z} + 4P_1 P_2 \bar{x} + 4P_1 P_3 \bar{y} + P_2^2 + P_3^2 = 1 , \quad (2)$$

where $z_i = x_i^2 + y_i^2$ , $\bar{z} = n^{-1}\Sigma_{i=1}^{n} z_i$ , $\bar{x} = n^{-1}\Sigma_{i=1}^{n} x_i$ , and $\bar{y} = n^{-1}\Sigma_{i=1}^{n} y_i$ .

Equations (1) and (2) can be posed in a matrix form:

$$F(\mathrm{I}_0) = \left\| \mathrm{M}_0 \mathrm{I}_0 \right\|^2 = \mathrm{I}_0^T (\mathrm{M}_0^T \mathrm{M}_0) \mathrm{I}_0 \quad (3)$$

where the superscript $T$ denotes the transpose of a matrix,

$$\mathrm{I}_0 = (P_1, P_2, P_3, P_4)^T \text{ and } \mathrm{M}_0 = \begin{bmatrix} z_1 & x_1 & y_1 & 1 \\ \vdots & \vdots & \vdots & 1 \\ z_n & x_n & y_n & 1 \end{bmatrix} \quad (4)$$

with the constraint $\mathrm{I}_0^T \mathrm{Q} \mathrm{I}_0 = 1$, and

$$\mathrm{Q} = \begin{bmatrix} 4\bar{z} & 2\bar{x} & 2\bar{y} & 0 \\ 2\bar{x} & 1 & 0 & 0 \\ 2\bar{y} & 0 & 1 & 0 \\ 0 & 0 & 0 & 0 \end{bmatrix} . \quad (5)$$

The minimization of the objective function $F(\mathrm{I}_0)$ can be achieved using the smallest nonnegative eigenvalue that corresponds to the generalized eigenvector of the matrix pair $(\mathrm{M}_0^T \mathrm{M}_0, \mathrm{Q})$ [11], [12]. With the solution $\mathrm{I}_0 = (P_1, P_2, P_3, P_4)^T$, the center $(x_c, y_c)$ and radius $R$ of the best-fitted circle can be recovered by

$$x_c = -\frac{P_2}{2P_1} , \; y_c = -\frac{P_3}{2P_1} , \text{ and } R = \frac{\sqrt{P_2^2 + P_3^2 - 4P_1 P_4}}{2|P_1|} . \quad (6)$$

*Edge Selection for Circle Fitting of the FH*

The front edge, which represented the first arrival of the echoes from the FH surface, was extracted as follows. The length from the center of the best-fitted circle to any point, **x** (**x** $\in \mathbf{\Gamma}$) was calculated. If the length was longer than the radius of the best-fitted circle, the point, **x** was considered from the first arrival. Otherwise, the point was discarded. Those admissible points were then used for a second circle fitting. The diameter of the best-fitted circle was then used as the estimated FH width, B.

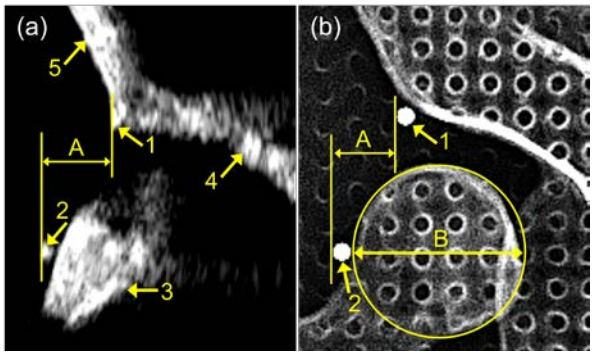


Figure 3. US and X-ray images of phantom 1. (a) The US coronal image shows the measurement of A, and (b) X-ray image shows the measurements of A and B. The annotation is as follows: 1. marker $i_1$, 2. marker $i_2$, 3. femoral head, 4. acetabulum, 5. edge of ilium.

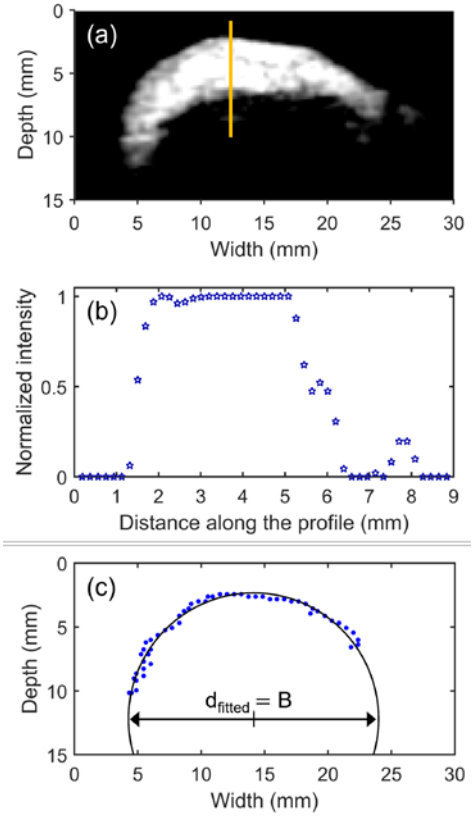


Figure 4. Circle fitting to the US image of the femoral head of phantom 1. (a) The US sagittal image of the femoral head and the line indicating the intensity profile of interest; (b) the corresponding normalized intensity profile; and (c) circle fitting to the front edge of the partial femoral head.

## II. Results

Fig. 3(a) shows the US images of phantom 1 after preprocessing with well visualized hip structures. The acetabular margin, lateral edge of the femoral head, and femoral head were clearly imaged on the coronal (Fig. 3(a)) and sagittal (Fig. 4(a)) views. Fig. 3(b) shows the AP X-ray image (of phantom 1) where A and B were measured.

TABLE I. AVERAGE MEASUREMENTS OF THE HEAD DISTANCE A, THE ESTIMATED WIDTH OF THE FEMORAL HEAD B, AND THE MP. THE ERROR WAS CALCULATED BY DIVIDING THE ABSOLUTE DIFFERENCE BETWEEN US OR X-RAY MEASUREMENTS AND 3D DESIGN MEASUREMENTS BY THE 3D DESIGN MEASURMENTS.

| | Quantity | 3D Design | US Measurement | US Error (%) | X-Ray Measurement | X-Ray Error (%) |
|---|---|---|---|---|---|---|
| Phantom 1 | $A_1$ (mm) | 6.98 | 7.19 | 3.01 | 7.24 | 3.72 |
| | $B_1$ (mm) | 19.45 | 19.6 | 0.77 | 19.54 | 0.46 |
| | $MP_1$ (%) | 35.89 | 36.68 | 2.20 | 37.05 | 3.23 |
| Phantom 2 | $A_2$ (mm) | 5.99 | 6.43 | 7.35 | 6.66 | 11.19 |
| | $B_2$ (mm) | 19.31 | 20.59 | 6.63 | 19.55 | 1.24 |
| | $MP_2$ (%) | 31.02 | 31.23 | 0.68 | 34.07 | 9.83 |

A line was drawn across the sagittal profile of the femoral head (Fig. 4(a)) and the corresponding normalized intensity profile is shown in Fig. 4(b) for phantom 1. The threshold for segmentation was set at 0.5 (50% of the peak pixel value). Fig. 4(c) shows the data points of the femoral head after edge selection and the best fitted circle.

The head distance (A) and FH width (B) were measured manually using a caliper on the 3D designs, the US images, as well as the X-ray images, and are summarized in Table I. All measurements were repeated 5 times except the calculated FH width ($B_1$ and $B_2$) on the US images. The maximum percentage error between the US measurements and the 3D designs were 7.35% for A, 6.63% for B, and 2.20% for MP, respectively. The corresponding values for X-ray measurements were 11.19 % for A, 1.24 % for B, and 9.83 % for MP, respectively.

## III. DISCUSSION

The main objective of this study was to establish the accuracy of US measurements using the 2D US images acquired by a handheld wireless US scanner. Using the 3D printed phantoms, our results have demonstrated for the first time that the calculated MP were accurate with 2.20% maximum error. On the contrary, the gold standard X-ray, whose accuracy has never been reported in literature, has an error up to 9.83%.

Feature identification, i.e., locating the acetabular margin and the lateral aspect of the FH in US images, is challenging. Phantom 1 had markers and thus rendered accurate head distance measurements. Phantom 2 had no markers and thus mimicked the clinical in vivo scanning. However phantom 2 incurred large measurement error for A (7.35%) even though the error was much smaller than the X-ray's (11.19%).

The large error in determining B was probably due to the small section of imaged FH surface available for circle fitting. In such a case, the algorithm might estimate a larger circle fitting, thus rendering a large estimation error. If a larger section was available, more accurate FH width estimation might be obtained. Another reason is that since the FH was not round and perhaps fitting by ellipses might be more appropriate. Further investigation should be performed in the future.

The threshold used in edge detection has notable effects on detecting the FH surface and eventually the estimation of the FH width. The threshold was used to discriminate the image from the background. A low threshold might include low intensity pixels that do not belong to the femoral head whereas a large threshold might detect boundary further inwards from its true boundary.

We also used a more objective best-fitting methodology to estimate FH width instead of the subjective manual method [9]. A fast least-squares based non-iterative solution was sought. In the future, a more accurate iterative method should be attempted to improve the accuracy.

While the experimental results favor the US method, this study has shown some limitations of the technique, which can be improved in our future work. More importantly, better scanning techniques and careful scanning operation will definitely improve the estimation process.

## IV. CONCLUSION

The phantom study has demonstrated a more accurate approach to estimate the MP from US images acquired using the more affordable 2D ultrasound technologies and without ionizing radiation. Using the phantom as reference, the US method was accurate up to 2.2% in comparison to 9.83% of the X-ray method. Clinical trials will be conducted to further validate the proposed US method.

## REFERENCES


[1] P. Rosenbaum, N. Paneth, A. Leviton, M. Goldstein, M. Bax, D. Damiano, et al., "A report: the definition and classification of cerebral palsy April 2006," *Dev. Med. Child. Neurol. Suppl*., vol.109, no.suppl 109, pp. 8–14, Feb. 2007.

[2] B. Soo, J. J. Howard, R. N. Boyd, S. M. Reid, A. Lanigan, R. Wolfe, et al., "Hip displacement in cerebral palsy,". *J. Bone Joint Surg*., vol. 88, no. 1, pp. 121-129, Jan. 2006.

[3] M. R. Bagg, J. Farber, and F. Miller, "Long-term follow-up of hip subluxation in cerebral palsy patients," *J. Pediatr. Orthop*., vol. 13, no. 1, pp. 32-36, Jan. 1993.

[4] N. H. Jung, B. Pereira, I. Nehring, O. Brix, P. Bernius, S. A. Schroeder, et al., "Does hip displacement influence health-related quality of life in children with cerebral palsy?," *Dev. Neurorehabil*., vol. 17, no. 6, pp. 420-425, Dec. 2014.

[5] M. Wynter, N. Gibson, K. L. Willoughby, S. Love, M. Kentish, P. Thomason, et al. "Australian hip surveillance guidelines for children with cerebral palsy: 5-year review," *Dev. Med. Child Neurol*., vol. 57, no. 9, pp. 808-820, Sep. 2015.

[6] J. Reimers, "The stability of the hip in children: a radiological study of the results of muscle surgery in cerebral palsy," *Acta Orthop. Scand*., vol. 51, no. sup184, pp. 1-100, July 1980.

[7] T. E. Terjesen, T. O. Rundén, and H. M. Johnsen, "Ultrasound in the diagnosis of congenital dysplasia and dislocation of the hip joints in children older than two years," *Clin. Orthop. Relat. Res*., vol. 262, pp. 159-169, Jan. 1991.

[8] A. Tegnander and T. Terjesen, "Reliability of ultrasonography in the follow-up of hip dysplasia in children above 2 years of age," *Acta Radiol*., vol. 40, no. 6, pp. 619-624, Jan. 1999.

[9] R. H. Kay, J. J. Noble, L. Johnston, S. F. Keevil, M. Kokkinakis, D. Reed, et al., "3D ultrasound to quantify lateral hip displacement in children with cerebral palsy: a validation study," *Dev. Med. Child Neurol*., vol. 62, no. 12, pp.1389-1395, Dec. 2020.

[10] A. Brahme A, *Comprehensive biomedical physics*. Newnes, 2014, pp. 153-168.

[11] N. Chernov, *Circular and linear regression: Fitting circles and lines by least squares*. CRC Press, 2010, pp. 121-127.

[12] G. Taubin, "Estimation of planar curves, surfaces, and nonplanar space curves defined by implicit equations with applications to edge and range image segmentation," *IEEE Comput. Archit. Lett*., vol. 13, no. 11, pp. 1115-38, Nov. 1991.